Laser-induced forward transfer of conductive nanoinks

Author: Blanca Mestre Torà
Facultat de Física, Universitat de Barcelona, Diagonal 645, 08028 Barcelona, Spain.

Advisor: Juan Marcos Fernández Pradas

Abstract: Laser-induced forward transfer (LIFT) is a noozle-free technique for printing materials presenting some advantages with respect to inkjet printing. LIFT of conductive nanoinks of high viscosity and particle content is explored in this work. The morphology and characteristics of the deposited material at different laser pulse repetition rates are analyzed. The improvement of electrical properties when applying several layers to the deposited material is studied, managing to obtain $R_s = 3.5\ m\Omega/\square$ when applying two layers. The gap dependence on the features of deposited material is investigated as well. Finally, as a proof of concept to develop electronic devices through LIFT of high viscosity inks, a resistance temperature detector is developed and characterized.

I. INTRODUCTION

New material transfer techniques for printed electronic approaches appear from the demand for manufacturing smaller and smaller electronic devices [1]. Nowadays, many techniques are available, being inkjet printing the most extended one. Such technique has some restrictions and limitations related to ink viscosity and size of the ink particles, as a nozzle is required [2]. Laser-direct write (LDW) is another material transfer method which has fewer limitations than inkjet printing as it is a nozzle-free technique. The most spread LDW approach is laser-induced forward transfer (LIFT) [2].

LIFT is utilized for transferring material from a carrier substrate covered with the donor layer to be deposited on the receiver substrate. Both substrates (carrier and receiver) are separated at a controlled distance, known as the gap. The transfer method consists of a laser beam focused in the interface between the carrier substrate and the donor layer. When a laser pulse impacts, the donor absorbs its energy causing the formation of an expanding bubble that produces a progressing jet. Eventually, this jet reaches the receiver when the laser pulse energy and the gap distance are arranged properly [3]. However, *Sopeña et al.* [2] observed that for high viscosity inks, samples are produced via the formation of an expanding bubble that forms a bridge when reaching the substrate. Figure 1 shows the schematic representation of the explained method.

Nowadays, there is an emerging urge for the industry to develop faster printing electronic techniques [5]. In this work, we analyze the impact of the laser frequency on the characteristics and morphology of the deposited materials through LIFT, which has not been explored in the past. Moreover, we investigate the influence of the gap on the features of the deposited material to obtain samples with the highest aspect ratio possible.

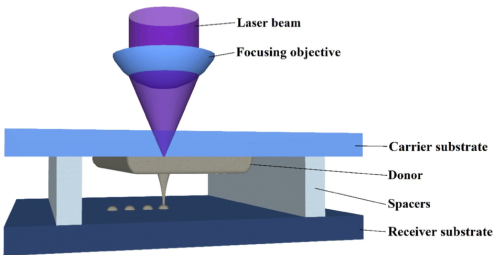

FIG. 1: Schematic representation of LIFT operation method. Image extracted from [4].

II. EXPERIMENTAL

A. Laser System

The laser printing system used to perform the experiments presented is a Q-switched Ytterbium-doped fiber laser (Rofin Powerline F20 Varia). It operates at the fundamental wavelength of 1064 nm, with pulses of 4 ns of duration. The laser has a galvo head attached which enables marking any pattern by moving the beam with speeds that range from 10 mm/s to 5 m/s. The laser beam has a Gaussian intensity profile and is focused with a beam waist of 20 μm using a 100 mm f-theta lens placed at the output of the galvo head.

The laser beam parameters, such as the speed of the beam, the repetition rate, the attenuation and the duration of the pulse, are controlled with the Visual Laser Marker program. The scanning mirrors move according to the pattern transferred through Visual Laser Marker program.

B. Sample preparation and deposition

A conductive paste of silver nanoparticles (XTPL, Ag nanopaste CL85) is used in the developed experiments. It consists on a non-Newtonian ink, its viscosity is $> 100\ Pa{\cdot}s$ and its density is 4.4 g/cm^3. This ink contains 85% of spherical silver nanoparticles and glycol as a solvent. Its nominal electrical resistivity is $4.2{\cdot}10^{-8}\ \Omega{\cdot}m$.

The donor substrate is prepared by spreading manually the ink onto a microscope slide. It has to be prepared carefully since the thickness has to be approximately 50 μm and as homogeneous as possible to undergo with the same printing conditions among the different parts of the sample.

Regarding the deposition process, a microscope slide acts as the receiver substrate. The distance of the donor substrate placed above the receiver substrate is controlled by a layer of fixed thickness (25 μm) placed between both substrates.

Once the ink is deposited at the receiver substrate, it is sintered in an oven for 30 minutes at 220 $^{\circ}C$ to optimize the electrical properties of the ink.

C. Sample characterization

The morphology analysis of the samples was accomplished through an optical (Carl Zeiss, model AX10 Imager.A1), a confocal microscope (Sensofar PLμ 2300) and SEM microscope (JEOL JSM-7001F). Electrical sample characterization was accomplished by a multimeter (Aim-TTi, model 1906).

III. RESULTS AND DISCUSSION

A. Frequency study

First, the study focuses on the deposited voxels morphology when working at different energies for each frequency. The frequencies we experiment with are 2, 10, 100, and 800 kHz. However, this fundamental study is not performed at 100 and 800 kHz as the maximum speed of the laser beam is 5 m/s, preventing the printing of separated droplets in these cases.

The minimum energy required to deposit droplets when working at 2 kHz is (11.4$\pm$0.3) μJ, obtaining radii of (29.1 $\pm$ 0.3) μm. When working at 10 kHz, the minimum energy necessary to print droplets is (16.1$\pm$0.5) μJ obtaining radii of (28.2$\pm$0.5) μm. This threshold energy phenomenon is due to the bubble. When it is formed at lower energies it does not reach the receiver as it turns back to the donor layer [2].

Figure 2a shows the squared radius of the deposited voxels for different energies. Notice that there is a linear dependence between these two quantities. In contrast, figure 2b shows their height, which is approximately constant in energy. Assuming that the voxels shape is a spherical cap, their volume has a linear energy dependence. This is an expected result since *Sopeña et al.* [2] observed linear dependence with voxels volume for increasing energies, which coincides with our observations.

Figure 2c shows how the aspect ratio of the voxels features decreases when rising the energy of the deposition process. In addition, 2 and 10 kHz aspect ratios coincide, showing similar values at most of the studied range of energies. However, for energy values near the threshold, the aspect ratios differ. Hence, we develop further printing studies working at energies near the threshold for each frequency as these correspond to the optimal conditions to deposit voxels with the highest aspect ratio.

We also develop a study for printing lines at different frequencies. This is due to the desire to achieve the optimal line printing conditions giving the lowest sheet resistance.

Lines are formed by overlapping droplets, i.e. decreasing the distance of the center of the voxels until they overlap and form continuous lines. This is done by working at the aforementioned energy conditions. Considering the lines printed at 100 kHz and 800 kHz, these conditions are determined through trial and error. Results show that 100 kHz printed lines require $E = (21.6 \pm 0.7)$ μJ while $E = (23 \pm 1)$ μJ is needed for 800 kHz.

As seen in figure 3a, which corresponds to the 2 kHz printing, as we increase the overlap to 80 μm a continuous line is obtained. As we decrease the spot separation a more uniform line is formed. When a voxel separation of 45 μm is reached, the lines become non-continuous until there is no ink deposition. This is unexpected, as when increasing the voxels overlap there should be more transferred material [6]. However, recent work from *Sopeña et al.* [2] reports a similar phenomenon when increasing the overlap of voxels of a non-Newtonian ink. To obtain continuous lines, the spot distance has to be equal or larger than the maximum bubble radius formed on the donor layer by the laser pulse. Otherwise, there would be a strong interaction between these bubbles, producing a non-continuous transfer of the layer [2].

Something similar is observed in figure 3b, where lines printed at 10 kHz with increasing overlap are shown. In this case, continuous lines are obtained when the spot distance reaches 80 μm. However, the non-continuous lines phenomenon appears at a distance of 60 μm.

When printing lines at a pulse repetition rate of 100 kHz (fig. 3c), continuous lines are obtained from 50 μm. This is the maximum allowed distance between pulses when working at this frequency. When increasing the overlap, a different phenomenon is observed. As we reduce the spot separation to 15 μm a *shattered* deposition is observed. A similar *shatter* phenomenon occurs in all lines printed at 800 kHz (fig. 3d), as lines have to be printed considering small voxel center distances due to laser speed limitation. This may be due to the short time and spatial distance between laser shots, causing that subsequent pulses impact in a forming bubble causing its shattering and spread in all directions. Nevertheless, this hypothesis is not proven and it could be studied in further research.

Figures 4a and 4b show how lines width slightly increases while their height diminishes when reducing the distance of the voxels centers. When analyzing the aspect ratio of deposited lines at different conditions (figure 4c), it is noticeable how it decreases when increasing the overlap in the droplets. We can conclude that the optimal spot distance is 65 μm for 2 kHz, 80 μm for 10 kHz, and 50 μm for 100 kHz.

The sheet resistance of the optimal deposited lines at each frequency is measured: $R_s = (6.6 \pm 0.6)$ $m\Omega/\square$ for 2 kHz, $R_s = (15 \pm 2)$ $m\Omega/\square$ for 10 kHz, $R_s = (10 \pm 1)$ $m\Omega/\square$ for 100 kHz.

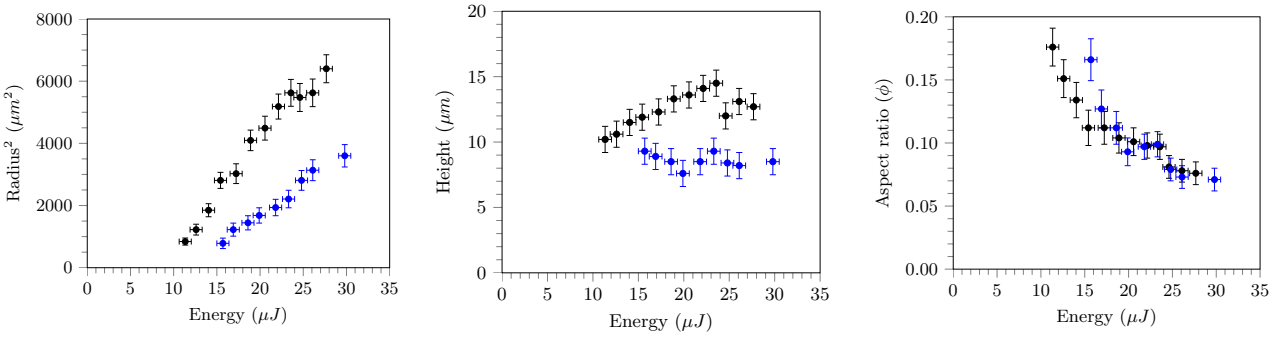

(a) (b) (c)

FIG. 2: Figure (a) shows squared radius of deposited voxels at different energies, (b) shows its height, and (c) shows aspect ratio of such voxels. Data corresponds to 2 kHz (•) and 10 kHz (•).

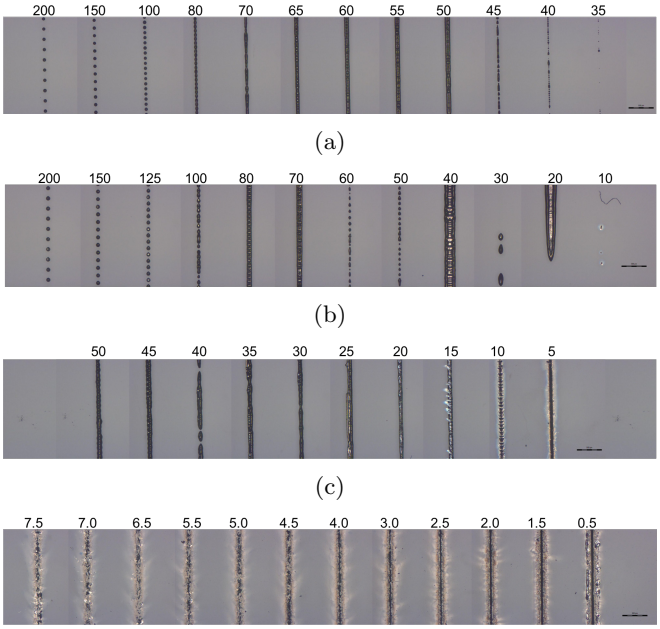

(a) (b) (c) (d)

FIG. 3: Optical images showing lines printed at (a) 2 kHz, (b) 10 kHz, (c) 100 kHz and (d) 800 kHz. Separation of voxels centers is specified above lines in μm. Scale bar corresponds to 500 μm.

B. SEM on the deposited lines

To analyze the morphology of the deposited lines, a SEM microscope is used. We compare the resulting lines before and after sintering to notice the association of the particles when the samples are treated at high temperatures.

In figure 5, the difference of the particles size between the non sintered and sintered samples is observed. Figure 5a corresponds to a non-sintered donor. It shows smaller clusters, whereas in figure 5b the size of the clusters is higher as they have been sintered and accommodated with the particles nearby [7].

Freq.	2 kHz		10 kHz		100 kHz	
# of layers	1	2	1	2	1	2
Width (μm)	50	75	80	100	60	105
Height (μm)	14	24	11	29	15	25
ρ ($\mu\Omega \cdot cm$)	10 ± 2	11 ± 1	16 ± 2	10 ± 1	15 ± 2	10 ± 1
R_s ($m\Omega/\square$)	6.6 ± 0.6	4.8 ± 0.4	15 ± 2	3.5 ± 0.2	10 ± 1	4.1 ± 0.3

TABLE I: Width, height and sheet resistance of the deposited lines when applying one or two layers. Width uncertainty is 3 μm, while height uncertainty is 1 μm.

Figure 6 shows SEM images of the LIFT deposited lines. It can be observed that such lines are homogeneous and uniform. Related studies using other inks rely on applying several layers to obtain uniform lines [2]. However, the nanoink used in our work requires only one layer to achieve even more satisfactory results.

When comparing 6a and 6b, we observe that the sintered line has a much more uniform surface than the non-sintered one, as through the sintering process the particles form higher nucleus, acquiring higher uniformity [7].

C. Double deposition

As seen in III B there is no need to apply several layers to accomplish uniform lines. Moreover, as seen in III A applying just one layer when printing, good line characteristics are obtained. Nevertheless, multiple layer deposition is performed to achieve even better results, aiming for lower sheet resistances. This study is performed for the following frequencies: 2 kHz, 10 kHz, and 100 kHz.

In table I we compare the size of the resulting lines and their electrical properties between printing once or twice. Even though their width expands when applying several layers, their height increases considerably, with almost no change in computed ink resistivity. Lines formed by applying one layer are already uniform and homogeneous (fig. 6). Thus, the decrease of the R_s is due to the increasing lines height.

When working at a laser frequency of 10 kHz a minimal value of sheet resistance is obtained. We manage to reduce the R_s from (15 ± 2) $m\Omega/\square$ to (3.5 ± 0.2) $m\Omega/\square$

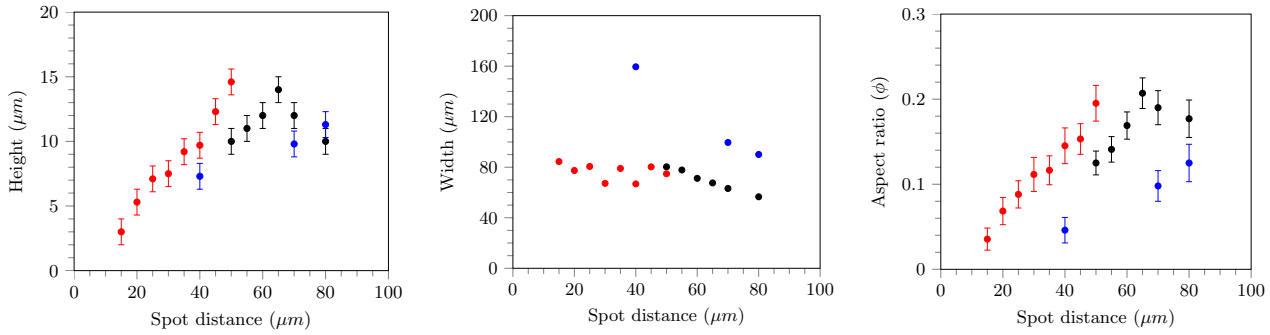

(a) (b) (c)

FIG. 4: Features of deposited lines. Figure (a) shows lines height while figure (b) shows lines width depending on the spot distance of the laser pulses. Standard deviation of lines width is 3 μm . Figure (c) shows lines aspect ratio. Data corresponds to 2 kHz (•), 10 kHz (•) and 100 kHz (•).

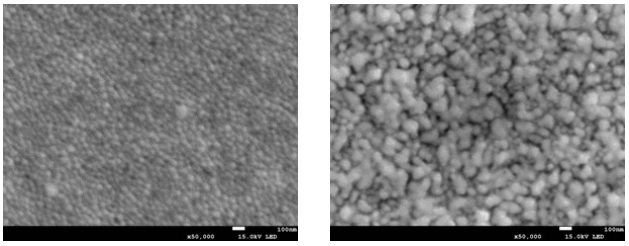

(a) (b)

FIG. 5: Image (a) corresponds to a non sintered ink while (b) to a sitenred ink. Images were acquired at ×50,000. Scale bar corresponds to 100 nm.

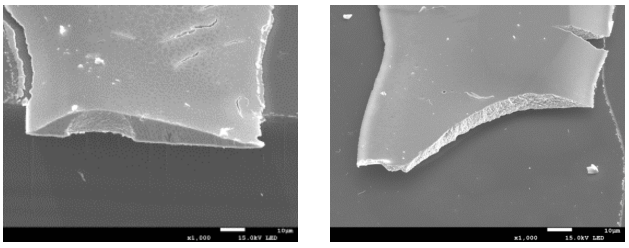

(a) (b)

FIG. 6: Image (a) corresponds to a non sintered line while (b) to a sitenred line. Images were acquired at ×1,000. Scale bar corresponds to 10 μm.

by applying a second layer.

D. Gap Study

When printing with the LIFT technique, an important variable that has to be controlled is the distance between the donor layer and the receiver substrate, as it has an impact on the morphology of the deposited material.

As shown in figure 7a, when increasing the distance between the donor layer and receiver, the width of the line diminishes. This result may occur as when the gap distance is larger, the formed bubbles have to advance a larger space to reach the substrate and form bridges. Consequently, this bubble has lower energy. Thus, the resulting bridges are thinner and the transferred material forms narrower lines.

In figure 7a, the width difference of the lines working at 2 kHz or 10 kHz is observed, where the lines printed at 10 kHz are slightly narrower. However, these differences decrease when approaching higher gap distances. The tendency may show that when reaching higher gap distances, lines printed at 2 kHz might become narrower than the ones printed at 10 kHz. This phenomenon would correspond with the results shown at table I when applying one layer. Nonetheless, this is a hypothesis that needs to be studied in further research.

Figure 7b shows the height of the printed lines, where no substantial changes are observed when varying the gap distance. However, the line printed at 2 kHz has a lower height, $\bar{h} = (9.3 \pm 0.5)\ \mu m$; while the one printed at 10 kHz has a height of $\bar{h} = (10.6 \pm 0.5)\ \mu m$. This way, the line height does not have a noticeable dependence on the gap. Nevertheless, in figure 7b it can also be observed that the line height has a certain irregularity from its nearly constant value. We may attribute this phenomenon to the irregular morphology of the donor layer as it is handcrafted, since lines height appears to have a noticeable dependence on such donor layer. This occurrence may justify the mismatch results shown in figure 7b and table I as they were obtained using different donor layers.

E. Proof of concept

To demonstrate the feasibility of the LIFT technique using high viscosity inks for developing functional devices such as measuring sensors, a resistance temperature detector (RTD) is printed and characterized.

The RTD is characterized by measuring the variation of its resistance by changing the environment temperature, from 22 $°C$ to 120 $°C$. For the calibration process, the RTD is placed in an oven and the RTD temperature is controlled using a thermocouple.

In figure 8 the impact of the temperature on the RTD

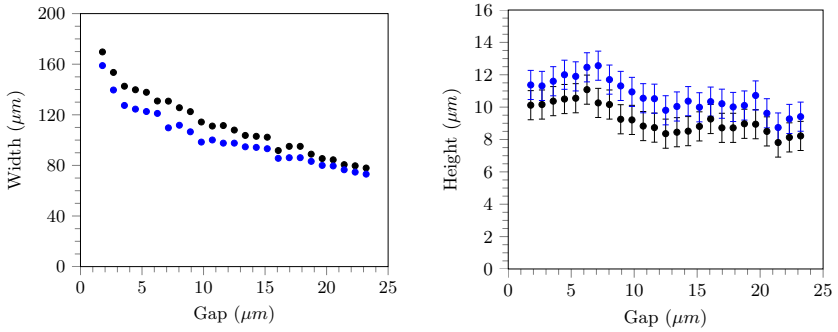

(a) (b)

FIG. 7: Features of deposited lines when varying the gap distance. Image (a) shows lines width while (b) shows its height. Width standard deviation is 3 μm. The dependences correspond to 2 kHz (•) and 10 kHz (•).

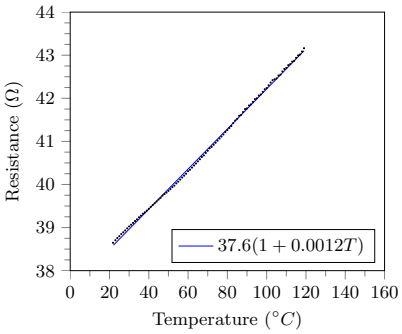

FIG. 8: Resistance variation with temperature. Experimental data (·) and linear regression (——) are shown. Resistance uncertainty is 0.05 Ω while temperature uncertainty is 0.1°C.

resistance is shown. As it can be observed, the resistance changes linearly with the temperature, following the next equation:

$$R(T) = R_0(1 + \alpha T) \tag{1}$$

where R_0 is the resistance at 0 °C and α the temperature coefficient. From equation 1 and figure 8 we can derive the R_0 of the resistance temperature detector, $R_0 = 37.6\ \Omega$. Moreover, we can determine RTD sensibility: $\alpha = 0.0012\ (^\circ C)^{-1}$. Such RTD has a lower sensibility compared to the most common used Pt100 RTD, which have $\alpha = 0.0038\ (^\circ C)^{-1}$. Nevertheless, our RTD is produced with a nanoink of silver, which is a cheaper material than platinum [8].

IV. CONCLUSIONS

- The feasibility of LIFT for conductive nanoinks of high viscosity has been proved. Moreover, we prove successful for printing at high frequencies (2 kHz, 10 kHz and 100 kHz) and implementing functional sensor devices.

- Good morphological characteristics and electrical properties are obtained for the depositions using this high viscosity nanoink. An improvement of these properties is observed when applying several deposition layers, managing to achieve a $R_s = (3.5 \pm 0.2)\ m\Omega/\square$ when applying two layers.

Acknowledgments

I thank Dr. J.M., Fernández-Pradas for the attention and advisory work. I also acknowledge my laboratory colleague E., Martí for all the advice at the laboratory. Many thanks to my family and friends for the unconditional support.

[1] Boutopoulos, C., Kalpyris, I., Serpetzoglou, E., and Zergioti, I. (2014). Laser-induced forward transfer of silver nanoparticle ink: time-resolved imaging of the jetting dynamics and correlation with the printing quality. Microfluidics and nanofluidics, 16(3), 493-500.

[2] Sopeña, P., Fernández-Pradas, J. M., and Serra, P. (2020). Laser-induced forward transfer of conductive screen-printing inks. Applied Surface Science, 507, 145047.

[3] Duocastella, M., Fernandez-Pradas, J. M., Morenza, J. L., and Serra, P. (2009). Time-resolved imaging of the laser forward transfer of liquids. Journal of applied physics, 106(8), 084907.

[4] Mikšys, J., Arutinov, G., and Römer, G. R. B. E. (2019). Pico-to nanosecond pulsed laser-induced forward transfer (LIFT) of silver nanoparticle inks: a comparative study. Applied Physics A, 125(12), 1-11.

[5] Rosa, P., Câmara, A., and Gouveia, C. (2015). The potential of printed electronics and personal fabrication in driving the Internet of Things. Open Journal of Internet Of Things, 1(1), 16-36.

[6] Palla-Papavlu, A., Córdoba, C., Patrascioiu, A., Fernández-Pradas, J. M., Morenza, J. L., and Serra, P. (2013). Deposition and characterization of lines printed through laser-induced forward transfer. Applied Physics A, 110(4), 751-755.

[7] Mo, L., Guo, Z., Yang, L., Zhang, Q., Fang, Y., Xin, Z., ... and Li, L. (2019). Silver nanoparticles based ink with moderate sintering in flexible and printed electronics. International journal of molecular sciences, 20(9), 2124.

[8] KING, Myke. Process control: a practical approach. John Wiley & Sons, 2016.